Available online at www.sciencedirect.com

ScienceDirect

journal homepage: www.elsevier.com/locate/issn/15375110

Research Paper

Optimisation of the filter housing dimensions of an automatic flushing strainer-type filter

Nicolas D. Cano [a], Antonio P. Camargo [b,*], Nassim Ait-Mouheb [c], Gustavo L. Muniz [d], Jhonnatan A.Y. Guarnizo [a], Diego J.S. Pereira [e], José A. Frizzone [f]

[a] Agricultural Engineering College, University of Campinas, Campinas, SP, 13083-970, Brazil
[b] Agricultural Engineering College, University of Campinas, Campinas, Brazil
[c] INRAE, UMR G-EAU, University of Montpellier, Avenue Jean-François Breton, 34000, Montpellier, France
[d] Agricultural Engineering College, University of Campinas, Campinas, SP, Brazil
[e] Biosystems Engineering Department, University of São Paulo, College of Agriculture "Luiz de Queiroz", Piracicaba, SP, Brazil
[f] Dept. of Biosystems Engineering, College of Agriculture "Luiz de Queiroz," Univ. of São Paulo, Piracicaba, SP 13418-900, Brazil

ARTICLE INFO

Article history:
Received 13 August 2021
Received in revised form
20 April 2022
Accepted 22 April 2022

Keywords:
Filtration
CFD
Screen filter
Irrigation engineering
Hydraulics

Filtration is essential in drip irrigation systems to remove physical contaminants carried by water that can clog the emitters, cause wear, or foul components of the system, affecting its performance and lifespan. Automatic flushing strainer-type filters initiate and terminate discrete flushing cycles that are activated automatically by means of differential pressure. The objective of this study is to investigate the hydraulic performance and flow behaviour of an automatic flushing strainer-type filter operated with clean water, using experimental and numerical approaches, to optimise the dimensions of its filter housing and to increase the range of operating flow rates. Pressure drop curves were determined for the filter housing and the filter system equipped with five models of filter elements (woven and non-woven elements). Excessive pressure drop in the filter housing and low filtration rates were identified as the main drawbacks of the original filter system. Numerical simulations enabled the identification of the most critical regions in terms of pressure losses near the transitions between the inlet and outlet segments of the pipe. Four designs of filter housing were simulated to evaluate the possibilities of optimising the filter housing dimensions using a constant filtering area. Larger inlet and outlet diameters combined to a filter housing shorter and wider were improvements in the filter housing dimensions that enabled to decrease the pressure drop in the filter and/or increase the range of operating flow rates. The results provided useful information for enhancing the hydraulic performance of the filtration system.

* Corresponding author.
E-mail addresses: n181139@dac.unicamp.br (N.D. Cano), apcpires@unicamp.br (A.P. Camargo), nassim.ait-mouheb@inrae.fr (N. Ait-Mouheb), gustavo.muniz@feagri.unicamp.br (G.L. Muniz), j261219@dac.unicamp.br (J.A.Y. Guarnizo), dpereira@usp.br (D.J.S. Pereira), frizzone@usp.br (J.A. Frizzone).

https://doi.org/10.1016/j.biosystemseng.2022.04.019
1537-5110/

Nomenclature

A	Total surface area of filtration (mm^2)
a, b	Fitted coefficients of the pressure drop equation
CFD	Computational fluid dynamics
D	Inlet diameter of the filter (mm)
D_{el}	Diameter of the filter element (mm)
D_{ho}	Diameter of the filter housing (mm)
h_{he}	Height of the filter element (mm)
h_{ho}	Height of the filter housing (mm)
NW	Nonwoven
PP	Polypropylene
Q	Flow rate ($m^3\ h^{-1}$)
q	Filtration rate ($m^3\ m^{-2}\ h^{-1}$)
Q_n	Nominal flow rate ($m^3\ h^{-1}$)
R^2	Coefficient of determination
SS	Stainless steel
y^+	Dimensionless wall distance
Δp	Differential pressure (kPa)
Δp_{exp}	Differential pressure for the original filter housing, obtained experimentally (kPa)
Δp_f	Differential pressure of the filter element (kPa)
$\Delta p_{housing}$	Differential pressure of the filter housing (kPa)
Δp_{sim}	Differential pressure for the original filter housing, obtained by numerical simulation (kPa)
Δp_{total}	Differential pressure of the filter system (filter housing and element) (kPa)

1. Introduction

Filtration involves the physical separation of one or more components from a suspension in a fluid by passage through or across a barrier (filter medium) that is permeable only to some of these components (Purchas & Sutherland, 2002). In irrigation systems, particularly in microirrigation, filtration is important to prevent the intake of particles and sediments that can accumulate along pipes and other components, resulting in the clogging of emitters. Under typical irrigation conditions, complete removal of all suspended particles cannot be achieved (ISO9912-1, 2004). Practical and economic limitations only allow for the removal of larger particles, and consequently, sediments can be found in irrigation lines (Oliveira et al., 2020; Puig-Bargués & Lamm, 2013; Ravina et al., 1992).

Strainer-type, or screen filters, are devices that contain one or more filter elements. The strainer-type filter elements consist of a perforated plate, screen, mesh, or a combination of these, intended to retain suspended solids larger than the aperture size specified by the manufacturer. The screen can be made of steel, nylon, polypropylene, or nonwoven materials. The material and characteristics of the screen directly affect the fluid flow and performance of the filter (Sparks & Chase, 2016; Sutherland, 2008). In irrigation applications, the filter performance mainly refers to hydraulic performance (i.e., pressure drop, filtration rate), removal efficiency of suspended particles, resistance to corrosion, and backwash effectiveness when automatic mechanisms are part of the filtration system. For woven wire cloths, the filtration performance is influenced by filter cloth specifications such as wire diameter, shape and material, type of weave (e.g., plain Dutch weave, twill Dutch weave, reverse Dutch weave), aperture size, and mesh count. The performance of nonwoven fabrics is influenced by the material, porosity, permeability, thickness, pore size, and mass per unit area of the fabric (Ribeiro et al., 2004, 2008). For media filters, the requirements for evaluating several characteristics related to filter performance are standardised in ASAE S539 (ASABE, 2017).

The filtration for irrigation systems may consist of primary and secondary filters. The primary filter may serve several plots and consist of a media filter, screen or disc filter, most often incorporating a self-cleaning mechanism. Screen or disc filters manually cleaned, can be installed as secondary downstream safety filters at the inlet of plots (Pizarro Cabello, 1996; Ravina et al., 1997). Screen filters are suitable for removing suspended solid particles, but problems may arise when algal debris are part of the contaminants. Algal material tends to intertwine between the screen mesh and removal is difficult when the packing becomes dense (Nakayama et al., 2007). If the irrigation water contains a high concentration of suspended solid particles, sand separators or settling basins should be installed upstream of the filtration system (Keller & Bliesner, 2000).

Some screen filters have flushing cycles that are automatically activated, and they are called automatic flushing strainer-type filters (ISO9912-3, 2013). Automatic flushing filters initiate and terminate discrete flushing cycles that are activated automatically by means of differential pressure or at regular intervals of time or filtered volume (Nakayama et al., 2007).

Several studies have emerged in recent years with the intention of improving designs for energy consumption, and understanding the flow behaviour and performance of filters, mainly media filters (Arbat et al., 2011; Bové, Arbat, Pujol, et al., 2015; Bové et al., 2017; Mesquita et al., 2019, 2017; Pujol et al., 2020; Solé-Torres et al., 2019). Many studies have used computational fluid dynamics (CFD) to investigate, design, and improve irrigation equipment (Camargo et al., 2020). Although experimental data will always be necessary for the validation of numerical simulations and to confirm the performance of irrigation equipment, numerical simulations can be useful to reduce resources related to development costs.

Mathematical models based on dimensional analysis have been developed to predict head losses of filters for irrigation systems operated with tap water (Yurdem et al., 2008, 2010), water with suspended solids, and effluents (Duran-Ros et al., 2010; Puig-Bargués et al., 2005; Zong et al., 2015). Some of these models can describe filter clogging as a function of the characteristics of the filter, water, and flow. CFD was used to estimate fluid flow characteristics and pressure losses in different parts of sand filters, as well as to propose improvements in the design of filter components aiming for better hydraulic performance (Arbat et al., 2011; Bové, Arbat, Pujol, et al., 2015; Mesquita et al., 2017, 2019). CFD studies on

strainer-type filters are scarce in the literature on irrigation engineering.

The objective of this study was to investigate the hydraulic performance and flow behaviour of an automatic flushing strainer-type filter operated with clean water, using experimental and numerical approaches, to optimise the dimensions of its filter housing and to increase the range of operating flow rates.

2. Material and methods

2.1. Filter

The automatic flushing strainer-type filter model FA-20 manufactured by Iavant Filtering Systems, Brazil, was investigated (Fig. 1). The filter housing is made of steel, and an electrostatic powder coating is applied over its inner and outer surfaces. The inlet and outlet internal diameters are 80 mm, and the total surface area of the filtration element is 272,376 mm^2.

This filtration system operates differently from other automatic flushing strainer-type filters. In this filter, the operating water flows from the outer to the inner surface of the filter element; thus, residues gradually accumulate over the external surface of the element. The automatic flushing mechanism is activated by a differential pressure threshold with a default value of 50 kPa. When the flushing routine is activated, the flushing valve is opened, and the electric motor coupled to a gearbox rotates the filter element. When the filter element rotates, its outer surface rubs against the brushes, which facilitates the detachment of solid material accumulated during the filtration routine. Parallel to the brushes, there is a narrow cavity that is connected to a flushing pipe. The differential pressure between the inside of the filter and the atmosphere is converted into a high velocity through the flushing pipe, which removes the material accumulated over the external surface of the filter element.

A technical description of the five models of the filter elements evaluated is presented in Table 1. According to the filter manufacturer, stainless steel (SS-120 and SS-150) and polypropylene (PP-120) models are used in several applications (e.g., irrigation, wastewater, water supply, and industry), whereas non-woven models (NW-500 and NW-2500) are usually required for industrial purposes. Figure 2 shows images of the woven and non-woven meshes obtained using a Leica M125C stereo microscope.

2.2. Experimental set-up

Tests were carried out at the Hydraulics and Irrigation Laboratory (LHI/FEAGRI/UNICAMP), Campinas, SP, Brazil.

The pressure drop curves as a function of flow rate were determined in the test bench, as illustrated in Fig. 3 using clean tap water. The hydraulically closed circuit consisted of a 25 m^3 water tank, a 18.6 kW centrifugal pump (maximum flow rate of 70 $m^3\ h^{-1}$ at 400 kPa), an orifice plate flow meter equipped with a differential pressure transmitter, calibrated in the range from 20 to 65 $m^3\ h^{-1}$ (maximum error of 5% from the measured value), a gate valve installed upstream of the filter to set the testing pressure, a temperature transmitter PT100 (0–50 °C, maximum error of 0.5 °C), a pressure transmitter (0–500 kPa, maximum error of 0.5% of the full scale), a differential pressure transmitter (0–100 kPa, maximum error of 0.5% of the full scale), the filter under test, and a gate valve installed downstream of the filter to adjust the test flow rate. The pressure tap distance was 5 *D* at the filter inlet and 10 *D* at the filter outlet (ASABE, 2017; ISO9644, 2008).

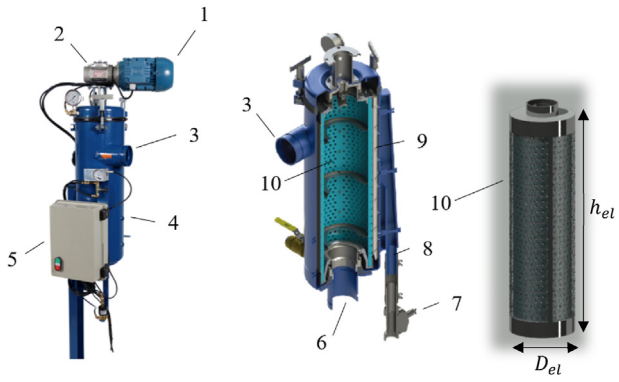

Fig. 1 – Automatic flushing strainer-type filter model Iavant FA-20. (1: electric motor; 2: gearbox; 3: filter inlet; 4: filter housing; 5: control panel; 6: filter outlet; 7: flushing valve; 8: flushing pipe; 9: flushing cavity and brushes; 10: filter element; D_{el}: diameter of the filter element; h_{el}: diameter of the filter element).

All sensors provided an analogue output signal that ranged from 4 to 20 mA, which varied linearly with the measured quantity. The data acquisition of all measurement instruments was performed using an electronic system equipped with a 16-bit analogue-to-digital converter to acquire analogue signals within the range of 4–20 mA and a resolution of 625 nA. The differential pressure was measured increasing and decreasing conditions of flow rate. For each test condition, 100 records of the sensor readings. were sampled at a 1 s acquisition interval. Data was gathered in three replications evaluating one unit of each filter element model.

Pressure drop curves as a function of flow rate were determined for the filter housing without filter elements, as well as for the filter system equipped with each of the filter elements shown in Table 1. The pressure drop in the filter was measured at flow rates varying from 25 to 65 $m^3\ h^{-1}$. The pressure at the filter inlet ranged from 350 to 400 kPa, and the average water temperature was 21.5 °C (20.7 and 22.5 °C were the extreme values). The automatic flushing mechanism was disabled during the experiments because it was not part of the purpose of this study.

2.3. Simulations evaluating the original filter housing

CFD simulations were performed to estimate the pressure drop of the original filter housing operated with clean water. In this stage, experimental data of pressure drop as a function of flow rate was available for comparison. Numerical simulations including filter elements were not included in this study.

The CFD module of COMSOL Multiphysics V. 5.4. was used to draw the three-dimensional solids representing the filter

Table 1 – Specifications of the filter elements provided by the mesh manufacturers.

Model	Material	Mesh count	Aperture size (μm)	Type of weave	Additional specifications
SS-120	Stainless steel	120	125	Plain Dutch weave	Wire diameter: 0.38 mm (warp) and 0.26 mm (weft); Number of apertures per inch: 24 (warp) and 110 (weft). Number approx. of apertures per cm 9 (warp) and 43 (weft)
SS-150	Stainless steel	150	100	Plain Dutch weave	Wire diameter: 0.23 mm (warp) and 0.18 mm (weft); Number of apertures per inch: 30 (warp) and 150 (weft). Number approx. of apertures per cm 12 (warp) and 59 (weft)
PP-120	Polypropylene	120	125	Satim weave, calendered, monofilament	Wire diameter: 0.64 mm; Mass per unit area: 300 g m^{-2}; Air permeability: 80 m^3 m^{-2} min^{-1} at 200 Pa
NW-500	Polypropylene	500	25	Non-woven, needlona® PP/PP 601	Air permeability: 13 m^3 m^{-2} min^{-1} at 200 Pa
NW-2500	Polypropylene	2500	5	Non-woven, needlona® PP/PP 604	Air permeability: 4 m^3 m^{-2} min^{-1} at 200 Pa

housing and running the numerical simulations. Simulations assumed an incompressible Newtonian fluid (i.e., water) and steady state conditions.

The realisable k–ε model was used to solve the turbulent flow. This model is an extension to the standard k–ε model which is used for simulating incompressible and single-phase flows at high Reynolds numbers (COMSOL Multiphysics, 2016). Comparison of turbulence models was not part of the study. Log-law wall functions were applied to approximate the flow velocity profile inside the boundary layer, serving to bridge the velocity profile from the wall to the main flow. The no-slip condition was assumed.

Simulations were performed for three flow rates corresponding to some of the conditions in which experimental data was available: 35.7, 49.5 and 62.8 m^3 h^{-1}. Taking the inlet diameter as a reference dimension, the Reynolds number varied from 162,099 to 285,149, indicating turbulent flow conditions in all simulations. The mean flow velocity corresponding to each flow rate was set as a boundary condition at the filter inlet, and the pressure was set to 400 kPa as a boundary condition at the filter outlet.

The mesh was generated based on the free tetrahedrals, including a boundary layer mesh (i.e., inflation or prism layer) near the walls (Fig. 4). The default values were kept for the boundary layer mesh (number of layers = 5; stretching factor = 1.2; thickness of first layer = automatic; thickness adjustment factor = 2.5).

The mesh quality was examined based on minimum and average element quality (skewness). Mesh independence analysis was performed to validate the simulations. Velocity profiles were plotted at four flow sections (inlet pipe, middle of the filter housing, outlet of the filter housing, and outlet pipe) and results of pressure drop in the filter were analysed to prove the results were mesh independent.

2.4. *Simulations for optimizing the filter housing dimensions*

Excessive pressure drop in the filter housing and low filtration rates were identified as the main drawbacks in the original filter system; hence, simulations focused on evaluating possibilities for optimizing the filter housing dimensions.

Four designs of the filter housing were simulated (Fig. 5). The total surface area of the filtration was kept constant in all the designs (A = 272,376 mm^2). The inlet and outlet diameters of the filter housing were the basic dimensions of the new designs and were set according to the commercial diameters of the steel pipes (80, 100, 125, and 150 mm).

The steps to obtain the main dimensions of the filter housing were as follows: 1) Define the inlet diameter (D); 2) Filter element diameter (D_{el}) = $D + 90$; 3) Filter housing diameter (D_{ho}) = $D_{el} + 40$; 4) Filter element height (h_{el}) = $\frac{A}{\pi D_{el}}$; 5) 5: Filter housing height (h_{ho}) = $h_{el} + 160$. The values summed to each of the variables were based on the dimensions measured in the original filter housing. Model A (80 mm) corresponded to the original filter housing dimensions, but inlet and outlet pipes were changed to 150 mm and reducing adapters were added, as explained below.

For optimising the filter housing dimensions, the maximum filtration rate 375 m^3 m^{-2} h^{-1} found in commercial

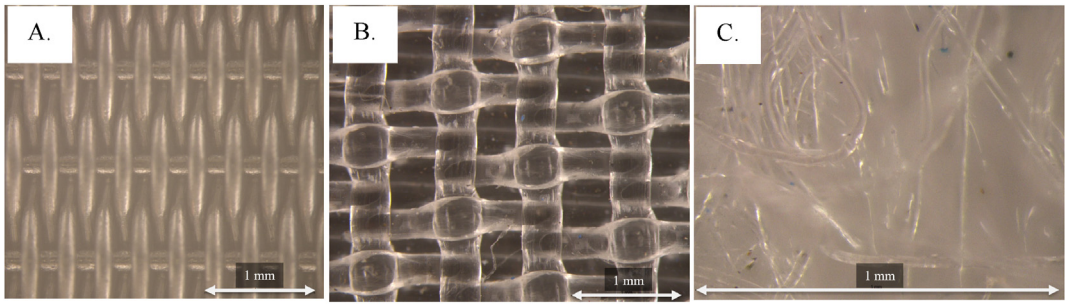

Fig. 2 – Evaluated meshes: (A) stainless steel plain Dutch weave (SS-120 and SS-150); (B) polypropylene satim weave (PP-120); (C) non-woven needlona (NW-500 and NW-2500).

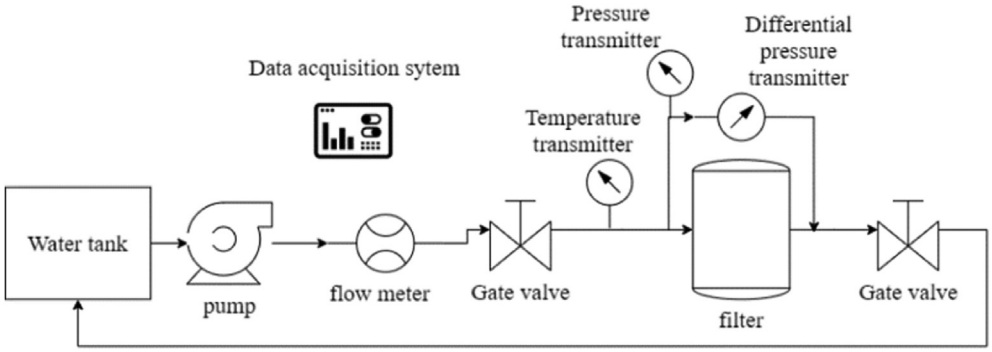

Fig. 3 – Test bench diagram.

automatic flushing strainer-type filters (AMIAD, 2022; AZUD, 2022; NETAFIM, 2022) was assumed as the target value (see discussion in section 3.1). For a total surface area of 272,376 mm^2, the corresponding flow rate for the automatic flushing strainer-type filter was 102.1 $m^3\ h^{-1}$. Therefore, a pressure of 400 kPa at the filter outlet and the flow rate of 100 $m^3\ h^{-1}$ were set as boundary conditions for CFD simulations. Also, pipes of 150 mm diameter and reducing adapters were included at the filter inlet and outlet in these simulations to keep flow velocities lower than 2 m s^{-1} in the pipeline, as recommended in most of practical applications (Azevedo Netto & Fernandez, 2015). Including the reducing adapters in the simulations enables to consider minor losses caused by these fittings.

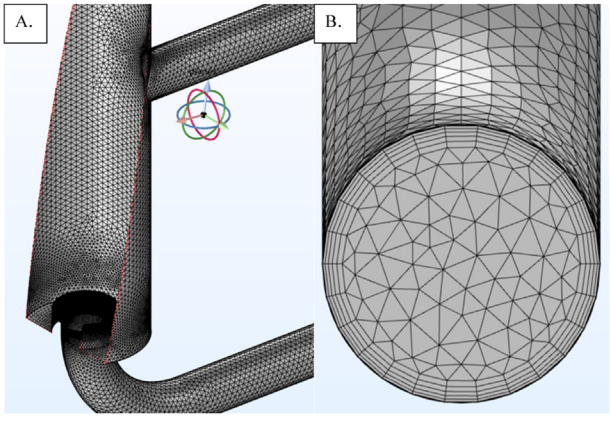

Fig. 4 – Mesh generated based on free tetrahedrals (A) including a boundary layer mesh near the walls (B).

3. Results and discussion

3.1. *Pressure drop curves – experimental data*

Figure 6 shows the pressure drop curves of the filtering system with and without the filter elements. The pressure drop curve in filters is influenced by the geometric characteristics of the filter housing and filter elements, as well as the filtering water characteristics (Wu et al., 2014). In this stage, the filter housing and filtering water quality were the same for all evaluations.

The pressure drop curves of the woven filter elements SS-120, SS-150, and PP-120 were similar. These three models offer similar resistance to flow, although Table 1 indicates differences in aperture size, wire diameter, wire material, and type of weave of these filter elements. Testezlaf and Ramos (1995) also found that the differences between pressure drop curves of 125- and 100-μm screen filters were not significant because of their similar permeability.

The pressure losses of 15 types of screen filters with plain weave woven wire cloth were analysed by Wu et al. (2014). The plain weave filter cloth is one of the simplest weave patterns, in which single wires (i.e., weft and warp wires) have the same diameter and are woven together to form rectangular or square apertures. Wu et al. (2014) developed an empirical model based on dimensional analysis to predict pressure losses in screen filters was proposed. In their experiments, the filter pore and the wire diameters ranged from 120.4 to

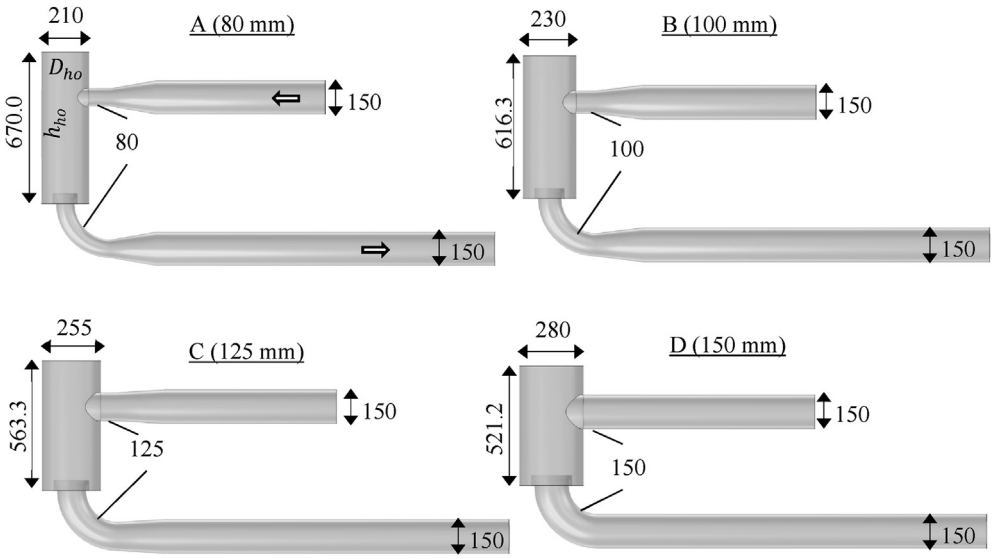

Fig. 5 – Main dimensions of the four models of filter housing simulated (dimensions in mm).

195.6 μm and 64.5–208.5 μm, respectively. For screen filters with 64.5 μm wire diameter, Wu et al. (2014) identified that the pressure drop increased when the mesh count was increased from 80 mesh to 140 mesh (i.e., the aperture size decreased from 200 to 115 μm), but the differences in pressure drop due to mesh count were not statistically significant. Also, for a given mesh count, the increase in wire diameter reduced the pore size and filter permeability and increased the pressure drop in the filters. Given a fixed flow range and mesh count, a larger inlet/outlet diameter and a thinner wire diameter of the screen reduced the inlet flow velocity and average filter flow velocity minimising both head loss caused by pipeline turbulence and local head loss caused by streams (Wu et al., 2014).

The pressure drop in a clean strainer-type filter ranges from 10 to 30 kPa, and the filter element should be cleaned when Δp reaches 40–60 kPa (Pizarro Cabello, 1996). In this study, the nominal flow rate (Q_n) for a clean filter was calculated assuming a midrange value of Δp, which was 20 kPa. The nominal flow rate ranged from 59.1 to 60.7 $m^3\ h^{-1}$ for the elements SS-120, SS-150, and PP-120 (Table 2). The difference in Q_n values among these elements was less than 5%.

The pressure drop curves of the non-woven filter elements (i.e., NW-500 and NW-2500) were stepper than those of the woven filter elements (i.e. SS-120, SS-150, and PP-120), which is expected because the non-woven elements presented lower permeability and offer higher resistance to flow than the

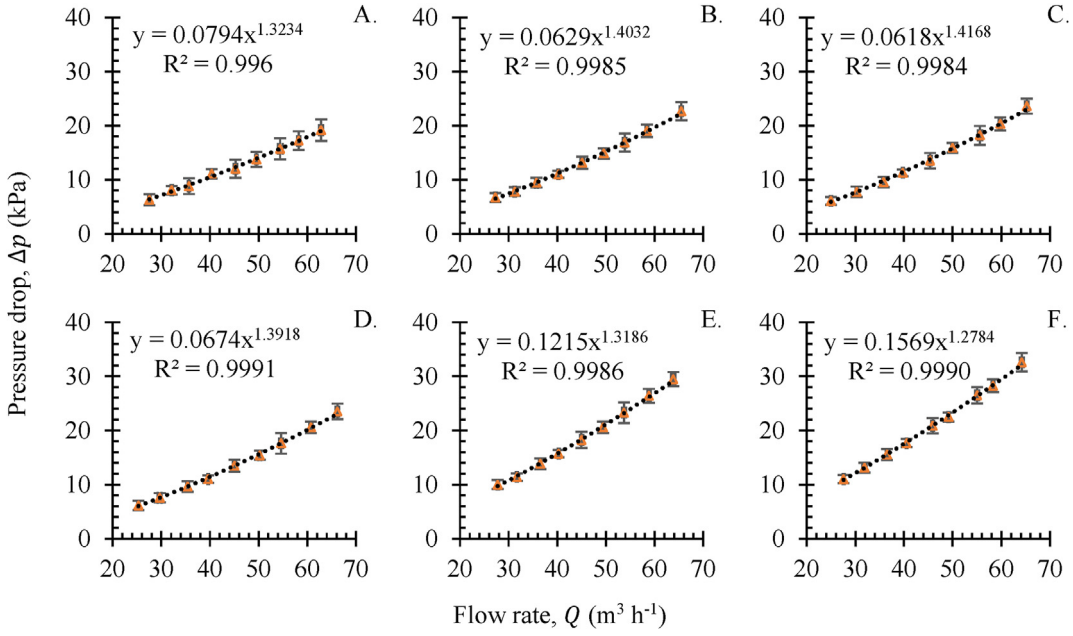

Fig. 6 – Experimental results of pressure drop curves of the filter housing and the filtering system equipped with each of the filter elements. (A) Filter housing; (B) SS-120; (C) SS-150; (D) PP-120; (E) NW-500; (F) NW-2500.

woven elements. The lower permeability of the non-woven elements also led to nominal flow rates that were approximately 20% smaller than those of the woven elements. Comparing the non-woven filter elements, the difference in Q_n was approximately 8%, although the air permeability of NW-500 was more than three times that of NW-2500.

At the nominal flow rate, the pressure drop due to the filter housing in the woven elements (i.e., SS-120, SS-150, and PP-120) was dominant and represented more than 87% of the total pressure drop in the filtering system (Table 2). In the non-woven filter elements operating at the nominal flow rate, the pressure drop due to the filter housing was more than 60% of the total pressure drop in the filtering system.

The percentages of pressure drop caused by the filter housing (Table 2) suggest that enhancements in the filter housing design could improve energy efficiency aspects and, perhaps, it could allow the filtering system to operate at higher flow rates (Demir et al., 2009; Wu et al., 2014). Table 2 presents the pressure drop equations for each filter element. These equations were estimated by the difference between the results of the total pressure drop in the filtering system and the pressure drop caused by the original filter housing.

In irrigation, the filtration rate of strainer-type filters with elements made of steel woven wire mesh usually range from 446 to 1004 $m^3\ m^{-2}\ h^{-1}$ (Pizarro Cabello, 1996). The flow rate can be obtained by multiplying the filtration rate by the total surface area of the filter element. For the stainless-steel elements evaluated (i.e., SS-120 and SS-150), the filtration rate at Q_n ranged from 217.0 to 222.9 $m^3\ m^{-2}\ h^{-1}$. The filtration rate values indicated in Table 2 are smaller than the values reported in the literature, which suggests that the filtering system could operate at higher flow rates if the filter housing design was improved to reduce the pressure drop. Based on the values presented by Pizarro Cabello (1996) for steel woven wire mesh, the flow rate values can vary from 121.5 to 273.5 $m^3\ h^{-1}$ (i.e., 446–1004 $m^3\ m^{-2}\ h^{-1}$).

If an increase in the flow rate does not interfere with the removal efficiency of solid particles, improvements in the filter housing design could contribute to enlarge the range of operating conditions of the filtration system, to reduce pressure losses and energy consumption. As examples to encourage further investigation on these aspects, the 4″ automatic vertical screen filter Netafim Screenguard™ exhibits a filtration surface area of 0.2 m^2 and maximum recommended filtration rate of 375 $m^3\ m^{-2}\ h^{-1}$ (NETAFIM, 2022); the 4″ Azud Luxon MFH 2400 M/4 has a filtration surface area of 0.24 m^2 and maximum recommended filtration rate of 375 $m^3\ m^{-2}\ h^{-1}$ (AZUD, 2022); and the 4" Filtomat M104C exhibits a filtration surface area of 0.212 m^2 and maximum recommended filtration rate of 377 $m^3\ m^{-2}\ h^{-1}$ (AMIAD, 2022). The maximum filtration rates recommended by the manufacturers of automatic flushing strainer-type filters are lower than the values proposed by Pizarro Cabello (1996). Regardless of the type of filter, lower filtration rates are recommended for low-quality water (Ravina et al., 1997).

3.2. Simulated and experimental pressure losses of the original filter housing

Simulations of the original filter housing were performed at flow rates of 35.7, 49.5 and 62.8 $m^3\ h^{-1}$. Mesh independence analyses were performed to validate all conditions simulated. Figure 7 shows velocity profiles plotted at four flow sections (I, II, III and IV) and results of pressure drop in the filter operating at 62.8 $m^3\ h^{-1}$, which corresponds to 3.47 m s^{-1} at the filter inlet. The influence of mesh size in the velocity profiles and values of pressure drop in the filter housing is clearly demonstrated in Fig. 7. Mesh independence was confirmed when the mesh size was increased from 4,053,468 (e) to 4,684,543 (f) elements. In these mesh sizes (e and f), the velocity profiles are practically matching at the four flow sections evaluated, and the pressure drop in the filter housing was 29.8 and 29.7 kPa, which represents a difference smaller than 0.5%. Although not shown here, the same procedure was used for proving the results were mesh independent in all CFD simulations.

Figure 7 also shows values of y^+ for the simulation at 62.8 $m^3\ h^{-1}$ using mesh size f, in which mesh independence was identified. The distance between the first grid cell and wall (y^+, dimensionless wall distance) should be lower than an upper limit, which depends on the Reynolds number (Pope, 2000). Log-law of wall provides a function for velocity to match the inner sub-layer to the outer layer and is extensively verified experimentally. The log-law wall functions are known to be valid for $30 < y^+ < 1000$ (Tabatabaian, 2015). In COMSOL, log-law is used for wall functions up to $y^+ = 11.06$ for the k-ε model and y^+ is designated by δ_w^+ in the software documentation (COMSOL Multiphysics, 2016; Tabatabaian, 2015).

In all simulations, the minimum element quality ranged from 0.065 to 0.1, and the average element quality varied

Table 2 – Nominal flow rate, filtration rate and percentage of pressure drop caused by the original filter housing when the filtering system is operating at the nominal flow rate, and pressure drop equation of each filter element.

Model	Q_n ($m^3\ h^{-1}$)	q ($m^3\ m^{-2}\ h^{-1}$)	% of pressure drop caused by the filter housing at Q_n	Pressure drop equation of the filter element $\Delta p_{f\,(kPa)} = a\ Q^b_{(m^3\ h^{-1})}$		
				a	b	R^2
SS-120	60.7	222.9	91.0	2.07E-5	2.79	0.992
SS-150	59.1	217.0	87.8	1.35E-4	2.41	0.997
PP-120	59.8	219.4	89.1	3.40E-4	2.15	0.999
NW-500	48.0	176.1	66.6	4.21E-2	1.31	0.999
NW-2500	44.4	162.8	60.0	8.08E-2	1.21	0.999

Q_n is the filtering system nominal flow rate predicted considering 20 kPa differential pressure; q is the filtration rate considering the total surface area of filtration and Q_n; Δp_f is the pressure drop of the filter element alone; Q is the flow rate; R^2 is the coefficient of determination.

between 0.68 and 0.72. In COMSOL, the mesh quality of 1 represents an optimal element quality, while minimum element qualities below 0.01 are very low quality and should be avoided to prevent convergence problems.

Figure 8 shows the experimental and simulated values of the pressure drop for the original filter housing evaluated under mean flow velocities at the filter inlet 1.97, 2.73 and 3.47 m s^{-1}, which corresponds to flow rates of 35.7, 49.5 and 62.8 m^3 h^{-1}, respectively. Simulations overestimated the pressure drop in the filter housing as the flow velocity was increased. Differences between measured and simulated values can be attributed to the simplifications in the three-dimensional model, inaccuracies of the turbulence flow model, and experimental data measurement uncertainty (Pope, 2000). Ilker and Sorgun (2020) observed errors of up to 20% evaluating the performance of different flow turbulence models for single-phase and liquid–solid slurry flows in pressurised pipe systems. Movahedi and Jamshidi (2021) evaluated the accuracy of different turbulence models for the prediction of pressure drop along with an annular pipe and reported errors of up to 25% according to the model employed. For practical purposes, to estimate how changes in the filter housing dimensions will influence the filter pressure drop, we can assume the prediction errors are acceptable and useful.

Part of the pressure drop found in filters is produced by the filter medium itself and cannot be avoided. However, a large

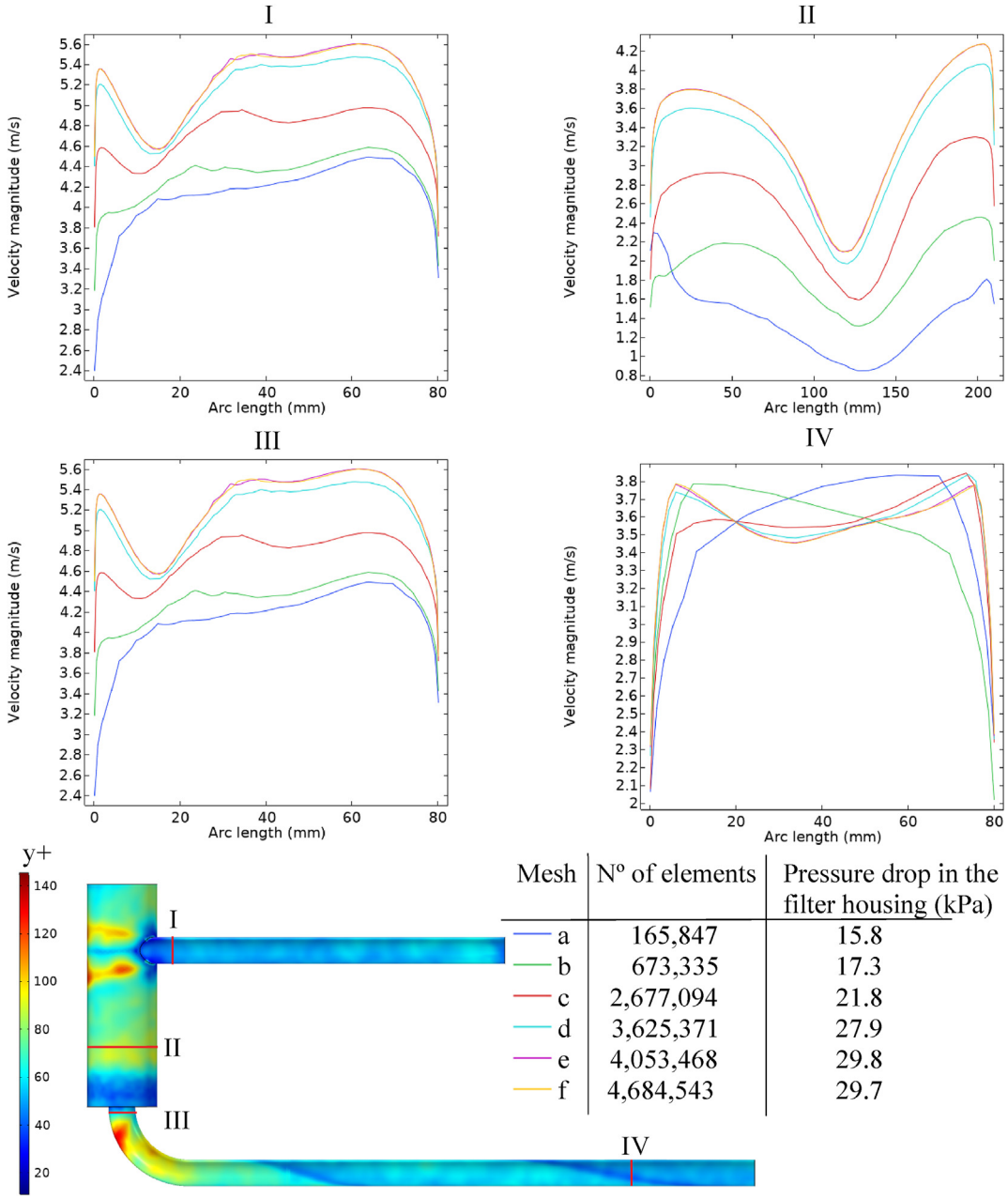

Mesh	Nº of elements	Pressure drop in the filter housing (kPa)
a	165,847	15.8
b	673,335	17.3
c	2,677,094	21.8
d	3,625,371	27.9
e	4,053,468	29.8
f	4,684,543	29.7

Fig. 7 – Velocity profiles at four sections (I, II, III and IV) of the original filter housing operating at 62.8 m^3 h^{-1}, pressure drop in the filter housing for each mesh size, and values of y^+ for mesh size "f" (4,684,543 elements) in which mesh independence of results was confirmed.

part of the pressure drop may be caused by the filter housing design and by auxiliary elements of the filter, and this could potentially be reduced without reducing the effectiveness of the filtration process (Bové, Arbat, Duran-Ros, et al., 2015). From the CFD simulations, the velocity streamlines and pressures were analysed to identify which regions of the filter housing caused most of the pressure drop. Figure 9 shows the results of the original filter housing simulated at 62.8 $m^3\ h^{-1}$ (i.e., mean flow velocity at the inlet = 3.47 $m\ s^{-1}$, outlet pressure = 400 kPa). Eight lines were positioned in the three-dimensional model, and the average pressure at each location was plotted (Fig. 9A). The most critical regions in terms of pressure losses (i.e., regions i and ii) are near the transitions between the inlet and outlet segments of the pipe (red dashed rectangles in Fig. 9A). These regions present sudden expansion (i) and sudden contraction (ii) of streamlines combined with the highest flow velocities (Fig. 9B). For the simulated condition, 37.6% and 46.2% of the pressure drop in the filter housing occurred from locations 2 to 3 (i.e., region i) and 5 to 6 (i.e., region ii), respectively (Fig. 9A). Thus, 83.9% of the total pressure drop in the filter housing occurred at regions i and ii. Improvements in filter housing seeking to reduce pressure losses should focus on changing the dimensions near regions i and ii. Bové, Arbat, Duran-Ros, et al. (2015) showed the importance of improving inlet/outlet regions and auxiliary elements of media filters. These authors proposed a new underdrain design and a packing strategy that could reduce the overall pressure drop in the filter by 35%.

The filter inlet is left aligned in the filter housing, which leads to the vorticity and circulation of water around the filter element. This position is important to avoid excessive strain on a small region of the screen and to allow a better distribution of impurities over the filtration element. A similar design of filter inlet was found for the 2" Spin Klin® disc filters – Amiad company (AMIAD, 2021).

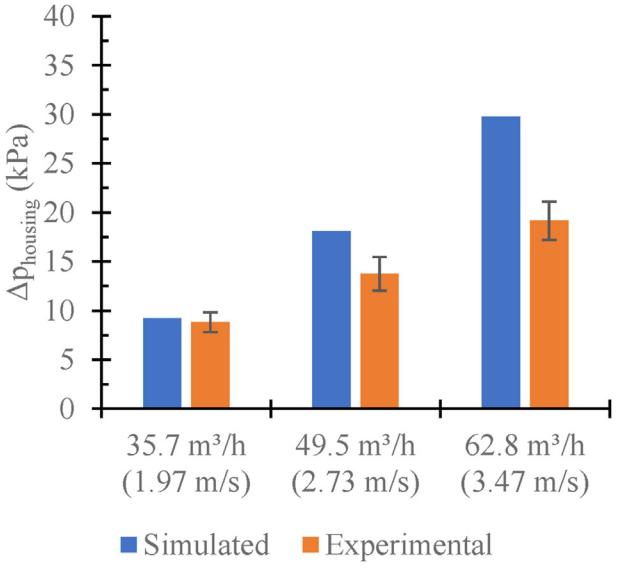

Fig. 8 – Simulated vs experimental values of pressure drop for the original filter housing at three operating conditions of flow.

In the current design of the filter housing, the highest flow velocities occurred at the inlet and outlet of the filter housing (Fig. 9B), leading to most of the pressure losses. The inlet and outlet sections should be enlarged to allow the filter to operate at higher flow rates with feasible pressure losses.

While sizing pipelines for irrigation applications, mean flow velocities higher than 2.0–2.5 $m\ s^{-1}$ are not recommended for operation of pressurised systems (Azevedo Netto & Fernandez, 2015; Frizzone et al., 2018; Lamm et al., 2007), but high velocities may occur in short segments of pipes and in its components. In general, excessive flow velocities increase pressure losses and energy waste, cause premature wear of components, and lead to more intense pressure surges in the case of water hammer events (Porto, 1999).

3.3. *Optimization of the filter housing dimensions*

The pressure losses in the filter housing designs simulated (Fig. 5) at 100 $m^3\ h^{-1}$ were: A (80 mm) = 57.6 kPa; B (100 mm) = 35.8 kPa; C (125 mm) = 25.8 kPa; D (150 mm) = 13.3 kPa. Following the same schema of locations illustrated in Fig. 9, the pressure losses were quantified for each of the proposed designs (Fig. 10). Increasing the dimensions at the inlet and outlet segments of the pipe (i.e., at the critical regions i and ii) effectively decreased the pressure drop in the filter housing. Because the allowable pressure drop in a clean strainer-type filter should be lower than 30 kPa (Pizarro Cabello, 1996), only designs C (125 mm) and D (150 mm) comply with the allowable pressure drop criterion at the target flow rate of 100 $m^3\ h^{-1}$ (q = 375 $m^3\ m^{-2}\ h^{-1}$).

A slight increase in pressure was observed between location 6 to 7 (Fig. 10). Although such small values are not relevant for practical purposes, it is known that pressure recovery downstream a 90° bend can be related to conversion between kinetic head and pressure head. A bend or curve in a pipe, as in the filter outlet, induces a pressure loss due to flow separation on the curved walls and a swirling secondary flow arising from the centripetal acceleration (White, 2011).

3.4. *Filter housing designs combined with filter elements*

CFD simulations combining filter housing designs with woven and non-woven filter elements were not possible in our current facilities. The arrangement, shape, and dimensions of the fibres in each type of filter element would result in a highly complex three-dimensional model that could not be simulated using the CFD module of COMSOL Multiphysics. Further investigation may take advantage of simulation tools such as GeoDict® filtration package, which has been developed particularly for the simulation of air and liquid filtration processes using woven and non-woven fabrics and meshes.

The experimental pressure drop equation shown in Table 2 assumes that the flow pattern obtained without the filter element (i.e., only the filter housing) is the same than that including it. But from Fig. 1, the installation of the filter element will modify the flow pattern, mainly at the filter inlet. Although flow behaviour and minor losses are influence by the presence of the filter element, the screen characteristics can be assumed to be the dominant factor when summing the pressure drop of the filter housing and filter element. A feasible method for

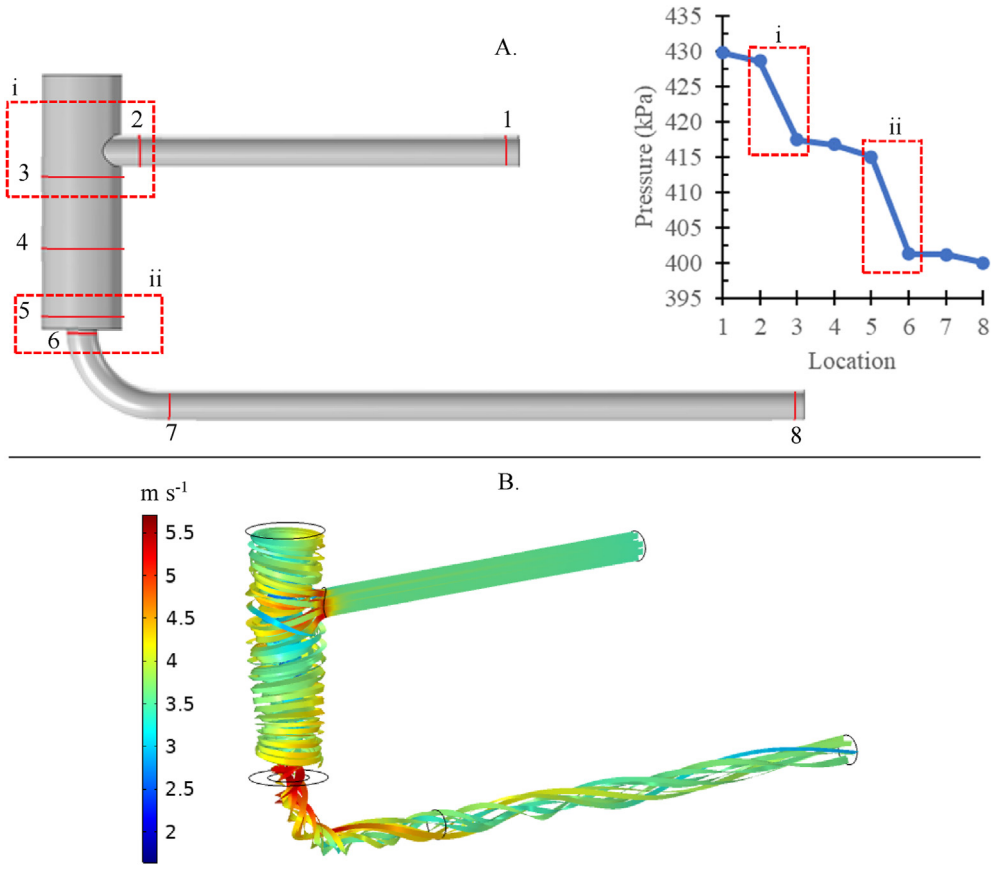

Fig. 9 – Simulation of the original filter housing at 62.8 $m^3\ h^{-1}$ (i.e., mean flow velocity at the inlet = 3.47 $m\ s^{-1}$). Average pressures at 8 locations and the most critical regions in terms of pressure loss, i and ii (A); velocity streamlines (B).

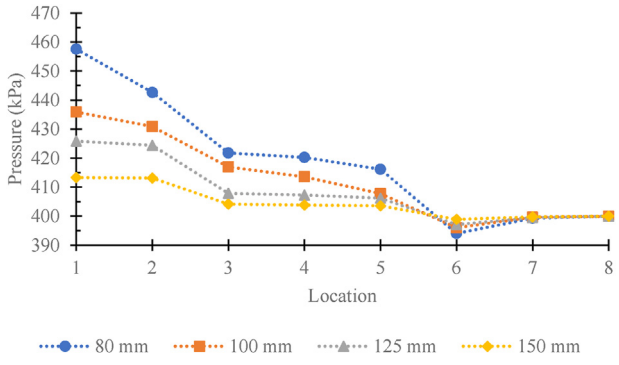

Fig. 10 – Pressure losses of four designs of the filter housing simulated with a target flow 100 $m^3\ h^{-1}$ ($q = 375\ m^3\ m^{-2}\ h^{-1}$).

approximating the pressure drop of the proposed filter designs and the existing filter elements consists of summing the pressure drop of each filter housing obtained from CFD with the pressure drop calculated from the equations of filter elements shown in Table 2. At this stage, simplifications and approximations must be performed to provide useful information before building new prototypes of the filter.

The best size of the filter housing depends on which is the target nominal flow rate defined by the manufacturer according to market strategies. Assuming a target flow rate of 100 $m^3\ h^{-1}$, Table 3 presents estimated operational characteristics of the filter housing designs equipped with the filter elements. The total pressure drop (Δp_{total}) was estimated by summing the pressure drop caused by the filter element (Δp_f) and the pressure drop in the filter housing, which was obtained from the CFD simulations.

Model A (80 mm) corresponds to the original filter housing coupled to inlet and outlet pipes of 150 mm diameter by reducing adapters (Fig. 5A). From Table 3, improvements in terms of pressure drop reduction for operation at 100 $m^3\ h^{-1}$ can be observed. Taking the model A as the reference for comparisons, for the filter equipped with the element SS-120, the decrease in pressure drop was 33.3, 48.5 and 67.6% for the designs B, C and D, respectively. For NW-2500, which presents the smallest permeability among the evaluated elements, the decrease in pressure drop was 27.6, 40.3 and 56.1% for the designs B, C and D, respectively.

In general, the woven wire filter elements (i.e., SS-120, SS-150, and PP-120) mounted within the filter housing D (150 mm) could operate at flow rates up to 100 $m^3\ h^{-1}$ with pressure drop lower than 30 kPa, which is a threshold mentioned by Pizarro Cabello (1996). Even the model C (125 mm) could be suitable since its values of Δp_{total} are near 30 kPa. Although the evaluation of the efficiency of suspended solids removal is not part of this research, the filtration efficiency is acceptable because the filtration rate values are matching the thresholds of commercial screen filters.

Table 3 – Estimated operational characteristics of the filter housing designs equipped with filter elements operating at 100 $m^3 h^{-1}$.

Filter element	Δp_f (kPa)	Model of filter housing			
		A (80 mm)	B (100 mm)	C (125 mm)	D (150 mm)
		Δp_{total} (kPa)			
SS-120	7.9	65.5	43.7	33.7	21.2
SS-150	8.9	66.5	44.7	34.7	22.2
PP-120	6.8	64.4	42.6	32.6	20.1
NW-500	17.6	75.2	53.4	43.4	30.9
NW-2500	21.3	78.9	57.1	47.1	34.6

The obtained results provide useful information for planning enhancements of the filtration system and for building prototypes for further experimental evaluation.

4. Conclusions

The hydraulic performance and flow behavior of an automatic flushing strainer-type filter operated with clean water were investigated using experimental and numerical approaches. For the original filtration system equipped with woven elements, the experimental results indicated that the pressure drop due to the filter housing was dominant and represented more than 86% of the total pressure drop in the filtering system. Similarly, for non-woven elements, more than 53% of the total pressure drop was caused by the filter housing. Excessive pressure drop in the filter housing and low filtration rates were identified as the main opportunities for improving the original filtration system.

CFD simulations were performed to predict values of pressure drop of the original filter housing operated with clean water. Numerical simulations enabled the identification of the most critical regions in terms of pressure losses near the transitions between the inlet and outlet segments of the pipe.

Keeping the filtering area constant, four designs of filter housing were simulated to evaluate possibilities for optimizing the filter housing dimensions. Larger inlet and outlet diameters combined to a filter housing shorter and wider were improvements in the filter housing dimensions that enabled to decrease the pressure drop in the filter and/or increase the range of operating flow rates. When comparing the proposed models of filter housing (models B, C and D) against the original design (model A) at the flow rate of 100 $m^3 h^{-1}$ (i.e., filtration rate of 375 $m^3 m^2 h^{-1}$), the decrease in pressure drop varied from 27.6% to 67.6% according to the combination of filter element and model of filter housing.

The CFD simulations indicates that the filter housing design of an existing automatic strainer-type filter can be improved to reduce pressure loss and/or increase the range of operating flow rates. The obtained results provide useful information for planning enhancements of the filtration system and for building prototypes for further experimental evaluation. The best size of the filter housing depends on the target nominal flow rate, which is defined by the manufacturer according to their market strategies. For development purposes, numerical simulations may reduce the number of prototypes manufactured for preliminary evaluations, thereby decreasing investment, time, and labour requirements.

Declaration of competing interest

The authors declare that they have no known competing financial interests or personal relationships that could have appeared to influence the work reported in this paper.

Acknowledgement

The authors would like to thank the Fundação de Amparo à Pesquisa do Estado de São Paulo [FAPESP-Brazil, Project 2018/20099–5] and Fundo de Apoio ao Ensino, Pesquisa e Extensão of the Universidade Estadual de Campinas [FAEPEX/UNICAMP Project No. 2022/19] for the financial support. We also appreciate the support of the Brazilian company IAVANT Sistemas de Filtragem for providing the equipment used in this investigation.

REFERENCES

AMIAD. (2021). *Spin Klin disc filter*. AMIAD. https://amiad.com/wp-content/uploads/2020/06/2-Spin-Klin-Catalogue-Irr-EN.pdf. (Accessed 10 February 2022).

AMIAD. (2022). *Filtomat self-cleaning screen filter*. https://amiad.com/wp-content/uploads/2020/06/Filtomat_A4_Irrig_En_2021-1.pdf. (Accessed 10 February 2022).

Arbat, G., Pujol, T., Montoro, L., Puig-Bargués, J., Duran-Ros, M., Barragán, J., & de Cartagena, F. (2011). Using computational fluid dynamics to predict head losses in the auxiliary elements of a microirrigation sand filter. *Transactions of the ASABE*, 54(4), 1367–1376. https://doi.org/10.13031/2013.39038

ASABE. (2017). *Media filters for irrigation - testing and performance reporting*. ASAE S539 (R2017).

Azevedo Netto, J. M., & Fernandez, M. F. (2015). *Manual de hidráulica* (9th ed.). São Paulo: Blucher.

AZUD. (2022). *Azud Luxon MFH*. https://azud.com/wp-content/uploads/2019/04/AZUD_LUXON_MFH-ENG.pdf. (Accessed 10 February 2022).

Bové, J., Arbat, G., Duran-Ros, M., Pujol, T., Velayos, J., Ramírez de Cartagena, F., & Puig-Bargués, J. (2015). Pressure drop across sand and recycled glass media used in micro irrigation filters. *Biosystems Engineering*, 137, 55–63. https://doi.org/10.1016/j.biosystemseng.2015.07.009

Bové, J., Arbat, G., Pujol, T., Duran-Ros, M., Ramírez de Cartagena, F., Velayos, J., & Puig-Bargués, J. (2015b). Reducing energy requirements for sand filtration in microirrigation: Improving the underdrain and packing. *Biosystems Engineering, 140*, 67–78. https://doi.org/10.1016/j.biosystemseng.2015.09.008

Bové, J., Puig-Bargués, J., Arbat, G., Duran-Ros, M., Pujol, T., Pujol, J., & Ramírez de Cartagena, F. (2017). Development of a new underdrain for improving the efficiency of microirrigation sand media filters. *Agricultural Water Management, 179*, 296–305. https://doi.org/10.1016/j.agwat.2016.06.031

Camargo, A. P., Muniz, G. L., Cano, N. D., Ait-Mouheb, N., Tomas, S., Pereira, D. J. de S., Lavanholi, R., Frizzone, J. A., & Molle, B. (2020). Applications of computational fluid dynamics in irrigation engineering. *Revista de Ciencias Agronomicas, 51*(5). https://doi.org/10.5935/1806-6690.20200097

Comsol Multiphysics. (2016). *CFD module user 's guide* (Vol. 598). COMSOL Multiphysics. https://doc.comsol.com/5.3/doc/com.comsol.help.cfd/CFDModuleUsersGuide.pdf. (Accessed 10 February 2022).

Demir, V., Yürdem, H., Yazgi, A., & Değirmencioğlu, A. (2009). Determination of the head losses in metal body disc filters used in drip irrigation systems. *Turkish Journal of Agriculture and Forestry, 33*(3), 219–229. https://doi.org/10.3906/tar-0811-1

Duran-Ros, M., Arbat, G., Barragán, J., Ramírez de Cartagena, F., & Puig-Bargués, J. (2010). Assessment of head loss equations developed with dimensional analysis for micro irrigation filters using effluents. *Biosystems Engineering, 106*(4), 521–526. https://doi.org/10.1016/j.biosystemseng.2010.06.001

Frizzone, J. A., Rezende, R., Camargo, A. P., & Colombo, A. (2018). *Irrigação por aspersão: Sistema pivô central*. Maringá: UEM.

Ilker, P., & Sorgun, M. (2020). Performance of turbulence models for single phase and liquid-solid slurry flows in pressurised pipe systems. *Ocean Engineering, 214*, 1–12. https://doi.org/10.1016/j.oceaneng.2020.107711

ISO9644. (2008). *Agricultural irrigation equipment — pressure losses in irrigation valves — test method*.

ISO9912-1. (2004). *Agricultural irrigation equipment — filters for micro-irrigation — Part 1: Terms, definitions and classification*.

ISO9912-3. (2013). *Agricultural irrigation equipment — filters for microirrigation — Part 3: Automatic flushing strainer-type filters and disc filters*.

Keller, J., & Bliesner, R. D. (2000). Sprinkle and trickle irrigation. *Caldwell*. The Blackburn press.

Lamm, F. R., Ayars, J. E., & Nakayama, F. S. (2007). *Microirrigation for crop production: Design, operation and management*. Amsterdam: Elsevier.

Mesquita, M., Deus, F. P., Testezlaf, R., Rosa, L. M., & Diotto, A. V. (2019). Design and hydrodynamic performance testing of a new pressure sand filter diffuser plate using numerical simulation. *Biosystems Engineering, 183*, 58–69. https://doi.org/10.1016/j.biosystemseng.2019.04.015

Mesquita, M., Testezlaf, R., Deus, F. P., & Rosa, L. M. (2017). Characterization of flow lines generated by pressurised sand filter underdrains. *Chemical Engineering Transactions, 58*, 715–720. https://doi.org/10.3303/CET1758120

Movahedi, H., & Jamshidi, S. (2021). Experimental and CFD simulation of slurry flow in the annular flow path using two-fluid model. *Journal of Petroleum Science and Engineering, 198*, 1–19. https://doi.org/10.1016/j.petrol.2020.108224

Nakayama, F. S., Boman, B. J., & Pitts, D. J. (2007). Maintenance. In F. R. Lamm, J. E. Ayars, & F. S. Nakayama (Eds.), *Microirrigation for crop production* (pp. 389–430). Amsterdam: Elsevier.

NETAFIM. (2022). Screenguard™ automatic screen filters. https://www.netafim.com/4ad930/globalassets/products/filters/screenguard/screenguard-automatic-screen-filter-product-page.pdf. (Accessed 10 February 2022).

Oliveira, F. C., Lavanholi, R., Camargo, A. P., Ait-Mouheb, N., Frizzone, J. A., Tomas, S., & Molle, B. (2020). Clogging of drippers caused by suspensions of kaolinite and montmorillonite clays. *Irrigation Science, 38*(1), 65–75. https://doi.org/10.1007/s00271-019-00652-4

Pizarro Cabello, F. (1996). *Riegos localizados de alta frecuencia* (3rd ed.). Madrid: Ediciones Mundi-Prensa.

Pope, S. B. (2000). *Turbulent flows*. Cambridge: Cambridge University Press.

Porto, R. M. (1999). In *Hidráulica básica* (2nd ed.). São Carlos: EESC-USP.

Puig-Bargués, J., Barragán, J., & Ramírez de Cartagena, F. (2005). Development of equations for calculating the head loss in effluent filtration in microirrigation systems using dimensional analysis. *Biosystems Engineering, 92*(3), 383–390. https://doi.org/10.1016/j.biosystemseng.2005.07.009

Puig-Bargués, J., & Lamm, F. (2013). Effect of flushing velocity and flushing duration on sediment transport in microirrigation driplines. *Transactions of the ASABE, 56*(5), 1821–1828. https://doi.org/10.13031/trans.56.10293

Pujol, T., Puig-Bargués, J., Arbat, G., Duran-Ros, M., Solé-Torres, C., Pujol, J., & Ramírez de Cartagena, F. (2020). Effect of wand-type underdrains on the hydraulic performance of pressurised sand media filters. *Biosystems Engineering, 192*, 176–187. https://doi.org/10.1016/j.biosystemseng.2020.01.015

Purchas, D. B., & Sutherland, K. (2002). *Handbook of filter media* (2nd ed.). Amsterdam: Elsevier Science & Technology Books.

Ravina, I., Paz, E., Sofer, Z., Marcu, A., Shisha, A., & Sagi, G. (1992). Control of emitter clogging in drip irrigation with reclaimed wastewater. *Irrigation Science, 13*(3), 129–139. https://doi.org/10.1007/BF00191055

Ravina, I., Paz, E., Sofer, Z., Marm, A., Schischa, A., Sagi, G., Yechialy, Z., & Lev, Y. (1997). Control of clogging in drip irrigation with stored treated municipal sewage effluent. *Agricultural Water Management, 33*, 127–137. https://doi.org/10.1016/S0378-3774(96)01286-3

Ribeiro, T. A. P., Paterniani, J. E. S., Airoldi, R. P. S., & Silva, M. J. M. (2004). Performance of non woven synthetic fabric and disc filters for fertirrigation water treatment. *Scientia Agricola, 61*(2), 127–133. https://doi.org/10.1590/S0103-90162004000200001

Ribeiro, T. A. P., Paterniani, J. E. S., Airoldi, R. P. S., & Silva, M. J. M. (2008). Comparison between disc and non-woven synthetic fabric filter media to prevent emitter clogging. *Transactions of the ASABE, 51*(2), 441–453. https://doi.org/10.13031/2013.24386

Solé-Torres, C., Puig-Bargués, J., Duran-Ros, M., Arbat, G., Pujol, J., & Ramírez de Cartagena, F. (2019). Effect of underdrain design, media height and filtration velocity on the performance of microirrigation sand filters using reclaimed effluents. *Biosystems Engineering, 187*, 292–304. https://doi.org/10.1016/j.biosystemseng.2019.09.012

Sparks, T., & Chase, G. (2016). *Filters and filtration handbook* (6th ed.). Waltham: Elsevier.

Sutherland, K. (2008). *Filters and filtration handbook* (5th ed.). Burlington: Elsevier.

Tabatabaian, M. (2015). *CFD module: Turbulent flow modeling*. New Delhi: Mercury learning and information.

Testezlaf, R., & Ramos, J. P. S. (1995). Sistema automatizado para determinação de perda de carga em filtros de tela e disco usados na irrigação localizada. *Pesquisa Agropecuária Brasileira, 30*(8), 1079–1088.

White, F. M. (2011). *Fluid mechanics* (7th ed.). New York: McGraw-Hill.

Wu, W., Chen, W. E. I., Liu, H., Yin, S., & Niu, Y. (2014). A new model for head loss assessment of screen filters developed with dimensional analysis in drip irrigation systems. *Irrigation and Drainage, 63*(4), 523–531. https://doi.org/10.1002/ird.1846

Yurdem, H., Demir, V., & Degirmencioglu, A. (2008). Development of a mathematical model to predict head losses from disc

filters in drip irrigation systems using dimensional analysis. *Biosystems Engineering, 100*(1), 14–23. https://doi.org/10.1016/j.biosystemseng.2008.01.003

Yurdem, H., Demir, V., & Degirmencioglu, A. (2010). Development of a mathematical model to predict clean water head losses in hydrocyclone filters in drip irrigation systems using dimensional analysis. *Biosystems Engineering, 105*(4), 495–506. https://doi.org/10.1016/j.biosystemseng.2010.02.001

Zong, Q., Zheng, T., Liu, H., & Li, C. (2015). Development of head loss equations for self-cleaning screen filters in drip irrigation systems using dimensional analysis. *Biosystems Engineering, 133*, 116–127. https://doi.org/10.1016/j.biosystemseng.2015.03.001